



HAL
open science

In-situ coupled mechanical/electrical investigations of EPDM/CB composite materials: The electrical signature of the mechanical Mullins effect

Clémentine Beutier, Laurent David, Guillaume Sudre, Philippe Cassagnau, Patrick Heuillet, Bernard Cantaloube, Anatoli Serghei

► **To cite this version:**

Clémentine Beutier, Laurent David, Guillaume Sudre, Philippe Cassagnau, Patrick Heuillet, et al.. In-situ coupled mechanical/electrical investigations of EPDM/CB composite materials: The electrical signature of the mechanical Mullins effect. *Composites Science and Technology*, 2022, 218, pp.109144. 10.1016/j.compscitech.2021.109144 . hal-03853905

HAL Id: hal-03853905

<https://hal.science/hal-03853905>

Submitted on 15 Nov 2022

HAL is a multi-disciplinary open access archive for the deposit and dissemination of scientific research documents, whether they are published or not. The documents may come from teaching and research institutions in France or abroad, or from public or private research centers.

L'archive ouverte pluridisciplinaire **HAL**, est destinée au dépôt et à la diffusion de documents scientifiques de niveau recherche, publiés ou non, émanant des établissements d'enseignement et de recherche français ou étrangers, des laboratoires publics ou privés.

In-situ coupled mechanical/electrical investigations of EPDM/CB composite materials: the electrical signature of the mechanical Mullins effect

Clémentine Beutier ^{a,b}, Laurent David ^a, Guillaume Sudre ^a, Philippe Cassagnau ^a,
Patrick Heuillet ^b, Bernard Cantaloube ^b, Anatoli Serghei ^{a,*}

^a *Univ Lyon, UCBL, CNRS, IMP UMR 5223, F-69622, Villeurbanne, France*

^b *LRCCP,94408 Vitry-sur-Seine, France*

Abstract

In-situ coupled mechanical/electrical investigations on EPDM-based composite materials prepared using CB fillers of different (low and high) structure and at different concentrations have been carried-out by cyclic and continuous loading, with simultaneous measurements of stress, strain and electrical conductivity. By investigations in dependence on the strain amplitude and unloading rate, the relationship linking the evolution of the electrical conductivity during mechanical deformation to the mechanical Mullins effect is demonstrated. A characteristic electrical signature accompanying the mechanical Mullins effect is revealed, originating from a kinetic reorganisation of the CB fillers by competing mechanisms of de-percolation and re-percolation. Notable differences between the electrical and the mechanical Mullins effect are also found, in particular, in relation to the kinetics of the stabilization of properties after the first mechanical deformation cycle. Our study brings new light into understanding the coupled evolution of mechanical and electrical properties of elastomeric composite materials, with possible applications in monitoring the material properties under mechanical deformation by in-situ electrical measurements.

Keywords: Smart materials; Mechanical properties; Electro-mechanical behaviour; Polymer-matrix composites (PMCs)

* Corresponding author: Anatoli Serghei
E-mail address: anatoli.serghei@univ-lyon1.fr

1. Introduction

Electrically conductive rubber composite materials are appropriate candidates for the development of a new generation of smart materials [1]. Due to their large deformation at break, impact resistance and flexibility, elastomers are a promising choice for the development of composite materials for sensor or actuator applications. In order to extend their range of applicability, in particular in the field of sensor applications, the electrical properties of elastomer matrix can be tailored by the incorporation of conductive particles. This type of conductive nanocomposite materials could have a great potential in the field of strain and damage sensing, with multiple applications in domains as different as health, automotive industry or electromagnetic interference shielding. The introduction of fillers into an elastomeric material significantly impacts its physical behaviour. Typically, this leads to an increase of the static and dynamic moduli [2] as well as to changes in other properties such as strength [3], fatigue resistance [4] and electrical conductivity [5]. The type and shape of fillers influence the viscoelastic behaviour of rubber materials [6]. For example, it is well known that an increased filler fraction in rubbers leads to both higher mechanical properties and mechanical hysteresis [7]. The deformation history plays an important role in the mechanical response of elastomers. This is best known through the manifestation of the softening phenomenon studied by Mullins and co-workers in the 1950s and known as the Mullins effect [8,9]. In the Mullins effect, deformation causes permanent changes in the elastomer microstructure, which influences the mechanical response of the material during subsequent deformations. As a consequence, a smaller stress is required to generate a given deformation in subsequent loadings, as long as the original deformation amplitude has not been exceeded. If the deformation amplitude exceeds the maximum amplitude previously reached, the stress needed to deform the material becomes independent of its

history and returns to a value close to that needed to deform a virgin specimen to the same strain [7,10]. Different micro-mechanical interpretations have been provided to explain this softening phenomenon, nonetheless, more than seven decades after the pioneering works of Mullins [8,9], the interpretation of the behaviour of such materials remains still a challenging task.

In-situ monitoring the evolution of the electrical conductivity under mechanical strain could represent an effective approach to identify permanent changes in the conductive rubber composite materials accompanying the Mullins effect. Different approaches have been followed to tune the conductivity-strain behaviour such as using different type of fillers [11], varying their aspect ratio [12] or employing polymers blends [13]. In most of the industrial applications, fillers are added to increase the mechanical properties of the rubber composites but some of the fillers, such as for instance carbon black (CB) or carbon nanotubes (CNTs), bring also enhanced conductive properties. Several authors investigated the evolution of the electrical behaviour of CB/polymer composites under cyclic loading [14–17] and viscoelastic relaxation phenomena but just few of them have pointed out “Mullins-like” hysteresis effects [15,17]. Among the few studies dealing with the phenomenon of electrical hysteresis in nanocomposite materials, De Focatiis *et al.* [15] reported that the resistivity-strain relationship for rubber materials exhibits a dependence on the history of the mechanical deformation. The observed resistivity-related hysteresis behaviour was associated to irreversible phenomena occurring in the conductive network. Zheng *et al.* [17] concluded that the correlation between the electrical resistance and mechanical strain for high-density polyethylene/CB composites depends on the structure of the matrix and that the electrical resistance is very sensitive to irreversible phenomena which occur within the polymer matrix. Some studies reported a non-monotonic resistance response, where a maximum of resistivity is observed during cyclic loading [15,17,18]. This behaviour is often explained by the

competition between destruction and reconstruction of the conductive network during cyclic loading and the time-dependent mechanical properties of the polymer matrix, but it is still not fully understood.

In the present work, an in-situ coupled mechanical/electrical approach is employed to correlate the evolution of electrical conductivity to the mechanical Mullins effect. This correlation opens the possibility of in-situ monitoring the mechanical properties of elastomeric composite materials by coupled electrical measurements. The essential advantage brought by the electrical measurements is their capacity of being easily implementable for materials working under real functioning conditions in an industrial environment. This can have potential applications in monitoring in real time the impact of fatigue, extreme deformations or damage on the material properties and functionality. In our study we demonstrate the deep relationship linking the evolution of the electrical conductivity during mechanical deformation to the mechanical Mullins effect. To this purpose, EPDM composite materials filled with CB fillers of different low and high structure and at different concentrations have been investigated. A clear electrical signature of the mechanical Mullins effect is evidenced. This characteristic electrical signature reveals a different facet of the mechanical Mullins effect, arising from a kinetic reorganisation of the CB fillers by competing mechanisms of de-percolation and re-percolation taking place parallel and perpendicular to the axial stretching direction. The evolution of the mechanical properties of elastomeric composite materials under mechanical strain can be thus correlated to the electrical conductivity, which can have potential applications in monitoring the impact of fatigue and damage of materials by in-situ electrical measurements.

2. Experimental

2.1 Materials

Experiments were carried out using Keltan EPDM rubber (Arlanxeo, Geleen, Netherlands) which is a semi-crystalline ethylene propylene diene monomer rubber with a density of 0.86 g.cm^{-3} and a Mooney viscosity $ML_{(1+4)}$ of 55 at $125 \text{ }^\circ\text{C}$. The EPDM was cross-linked using different amounts of low structured (LS) carbon black (N326) or highly structured (HS) carbon black (N347) fillers with sulphur bridges. CB N326 and N347 were provided by Orion (Frankfurt, Germany). Elastomer composites of different compositions were obtained, as specified in Tab. 1. The processing oil selected as plasticiser was Torilis 6200, provided by Total (Ferrybridge, UK).

Table 1. Composition of EPDM in %_{vol} where LS mean low structured (N326) and HS highly structured (N347) CB fillers. The vulcanization time $t_{98\%}$ (determined by MDR) and the density of the composite compounds are also reported.

	<u>Density</u>	<u>EPDM-25LS</u>	<u>EPDM-25HS</u>	<u>EPDM-35LS</u>
EPDM	0.86	60.0	60.0	52.5
CB	1.8	25.5	25.5	35
Oil Torilis 6200	0.89	11.5	11.5	10
ZnO / stearic acid	5.57 / 0.85	1.1	1.1	0.5
Accelerators	-	0.5	0.5	0.5
Sulfur	2.1	0.7	0.7	1
Antioxidant: TMQ	1.1	0.7	0.7	0.5
Vulcanization: $t_{98\%}$ (min)	-	16	15	13

2.2 Sample preparation

The sample preparation was done in tree steps. The 1st step was to blend the elastomer, the processing oil and the CB fillers in an internal batch mixer (Banbury 3.2 L)

at the temperature of 60 °C at 60 rpm for around 4 min. The 2nd step was to add and mix the vulcanisation systems (sulphur, accelerator, activator and antioxidant) with the blend obtained at step 1, using a two-roll mixing mill (Agila, roll dimensions: 300 x 700 mm) at 60 °C with a velocity of 20 rpm for 5 min. The last step was to measure the kinetics of vulcanization for each composite at 170 °C using a moving die rheometer (MDR one, TA instruments). The time to reach 98 % of vulcanized network $t_{98\%}$ was measured as illustrated in the Supplementary Information Part (Fig. S1). Then, slabs of rubber were vulcanized during press moulding at 200 bar and 170 °C for a time period equal to $t_{98\%}$, as reported in Tab. 1.

2.3 Mechanical measurements

Uniaxial tensile testing and cyclic loading were performed using a Shimadzu AG-X+ testing machine at room temperature and constant crosshead displacement velocity of 10 mm/min. Specimens were cut with a dumbbell cutting die at the following dimensions: $30 \times 4 \times 2 \text{ mm}^3$. The true strain ε is calculated as $\varepsilon = \ln(1 + \Delta L/L_0)$, where L_0 is the gauge length and ΔL is the crosshead displacement corresponding to the undeformed state and $\varepsilon_{nom} = \Delta L/L_0$. The nominal stress, σ_{nom}^{mec} is defined as $\sigma_{nom}^{mec} = F/S_0$, where F is the measured force and S_0 is the initial cross-sectional area of the specimen. Considering iso-volume deformation conditions (Poisson coefficient equal to 0.5), the true stress σ^{mec} can be expressed as $\sigma^{mec} = \sigma_{nom}^{mec}(1 + \varepsilon_{nom})$.

The experiments to investigate the mechanical properties of our materials were performed using two different approaches. The 1st approach was to apply a continuous deformation until failure. The 2nd one was to perform 50 cycles at true deformation amplitudes reaching ε_{max} of 0.09, 0.18, 0.35, 0.47, 0.57, 0.69 and returning to ε_{min} values

corresponding to complete unloading ($F = 0$). The strain evolution with time for these types of experiments is presented in the Supplementary Information Part (Fig. S2a-b).

2.4 Electrical measurements

The electrical properties of our composite materials in an equilibrated state were measured at room temperature after a thermal treatment of at least 1h at 140 °C under vacuum. The samples were cut in strips of $40 \times 15 \times 2 \text{ mm}^3$. The electrical contacts were gold metallized by sputtering in order to eliminate the influence of the contact resistance. The electrical conductivity was measured using a Novocontrol Alpha Broadband Dielectric/Impedance Spectrometer (BDS) in the frequency range from 10^5 Hz to 10^0 Hz . As shown in the Supplementary Information Part (Fig. S3), a thermal treatment of 1 h is necessary in order to obtain a rejuvenated sample which shows a negligible impact of previous mechanical history and ageing. Typical conductivity measurements by BDS are shown in the Supplementary Information Part (Fig. S4). In a broad frequency range, a conductivity plateau independent of frequency is detected, corresponding to the DC-conductivity of the samples under study. **Experiments were also carried-out under a DC-field, using a Keysight B2980A picoammeter. The comparison between the DC and the AC measurements (taken at a frequency that corresponds to the DC-plateau) led to identical results. This indicates that the structure of the electrodes and the electrical contacts play a negligible role in our experiments.** The conductivity-concentration curves for EPDM/CB composites filled with LS CB and HS CB are shown in Fig. 1. The percolation curves indicate that our materials become conductive at about 13%vol of CB, for both LS and HS fillers. Given the large statistical variations in the static conductivity for filler concentrations close to the percolation threshold (as shown in the Supplementary Information Part, Fig. S5), our study focused on materials with filler concentrations as

high as possible. Therefore, EPDM-25LS, EPDM-25HS and EPDM-35LS have been chosen to carry-out the coupled mechanical/electrical investigations. Above these concentrations, the material processing is not any longer possible. The mechanical and electrical properties of the investigated EPDM/CB nanocomposite materials are reported in the Supplementary Information Part (Tab. S1).

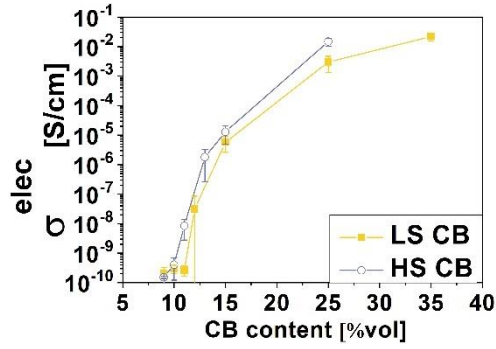


Figure 1. Electrical conductivity as a function of the CB concentration in %vol for low and highly structured CB fillers.

2.5 In-situ coupled mechanical/electrical investigations

The measurement set-up for in-situ coupled mechanical/electrical investigations is illustrated in Fig. 2. The specimens are fixed between a polycarbonate piece and brass electrodes by four screws. The polycarbonate piece is designed to fit into the tensile testing grip of the Shimadzu instrument. The set-up for coupled measurements was tested and validated by comparing the obtained mechanical σ^{mec} vs. ϵ curves to the results measured by using the standard Shimadzu grip (Supplementary Information, Fig. S6). The electrical conductivity σ^{elec} was determined by taking into account the variation of the geometry of specimens during the tensile test, using the formula $\sigma^{elec} = \frac{L}{R \times S}$, where L represents the sample length, S the sample cross section and R the electrical resistance measured by the Keysight B2980A picoammeter at 5 V. The experimental setup

presented in Fig. 2 was used to characterize the evolution of the electrical and mechanical properties of EPDM/CB composites as a function of strain.

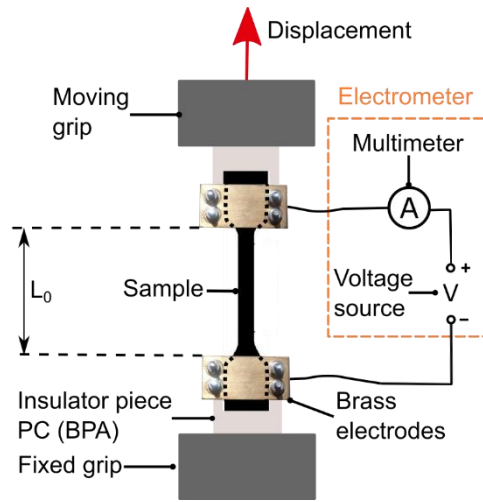


Figure 2. Schematic representation of the setup used for carrying-out coupled mechanical/electrical investigations.

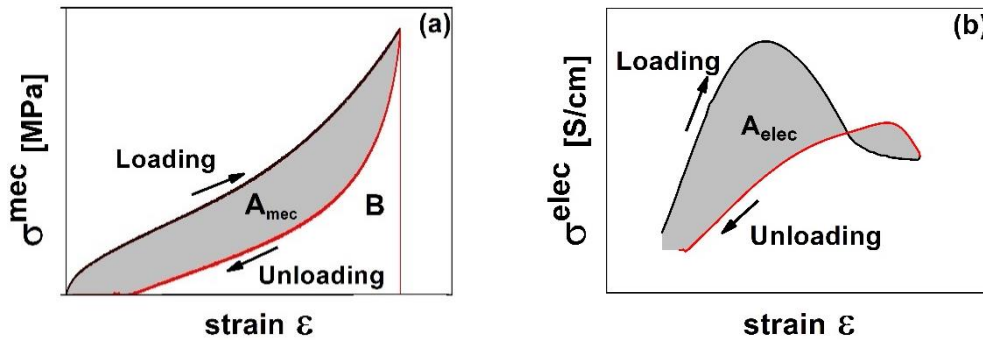


Figure 3. Definition of the Mullins ratio R_M representing the energy fraction that is dissipated during one stress-strain cycle. A_{mec} represents the area between the loading curve and the unloading curve which characterizes the dissipated energy. B represents the area under the unloading curve. The electrical hysteresis A_{elec} represents the area between the loading and the unloading conductivity curve.

The mechanical hysteresis associated with the Mullins effect can be quantified as the ratio between the dissipated mechanical energy (area of the hysteresis) and the energy

of the first loading (area below the loading of the virgin material): $R_M = \frac{A_{mec}}{A_{mec}+B}$ where A_{mec} is the area between the loading and the unloading curves and B is the area under the unloading curve. Fig. 3a shows a typical example for the evaluation of the Mullins ratio R_M for a given applied strain. Furthermore, the phenomenon of electrical hysteresis has been systematically compared to the mechanical hysteresis. A typical example of an electrical hysteresis over the first loading, calculated as the area A_{elec} between the loading and the unloading curve, is given in Fig. 3b.

3. Results and discussion

3.1 Mechanical Mullins effect

Regardless of the filler concentration or structure, after the first cycle the maximum σ^{mec} corresponding to ε_{max} decreases for the following cycles and reaches a constant σ^{mec} after 4 cycles, as shown in the Supplementary Information Part (Fig. S8). Hence, the stabilization of the mechanical properties takes around four cycles to be achieved. All studied materials exhibited the Mullins effect, as reported in Fig. 4. The second and subsequent cycles exhibit stress-softening: upon loading, the σ^{mec} is significantly lower as compared to the first cyclic loading at the same ε . Once the previous ε_{max} has been exceeded, the σ^{mec} tends to return to a value close to the value that would be measured in a single continuous loading of a virgin sample, i.e. as if the previous cycles never occurred. For EPDM-25HS, the stress upon cyclic deformation does not return to the exact value obtained by the continuous curve. This is due to relaxation phenomena, expected to play an important role when the time-scale of the reorganisation kinetics of the composite material upon loading/unloading is slower or comparable to the time-scale imposed by the unloading rate.

Comparing the mechanical properties of the EPDM/CB composites, it is observed that the σ^{mec} obtained at a given ϵ is higher for composites filled with HS CB fillers than for composites filled with LS CB (Fig. 4a and 4b). Furthermore, the σ^{mec} is increasing with the filler content (Fig. 4a and 4c). The mechanical properties of the composite materials investigated in our study are summarized in the Supplementary Information (Tab. S1).

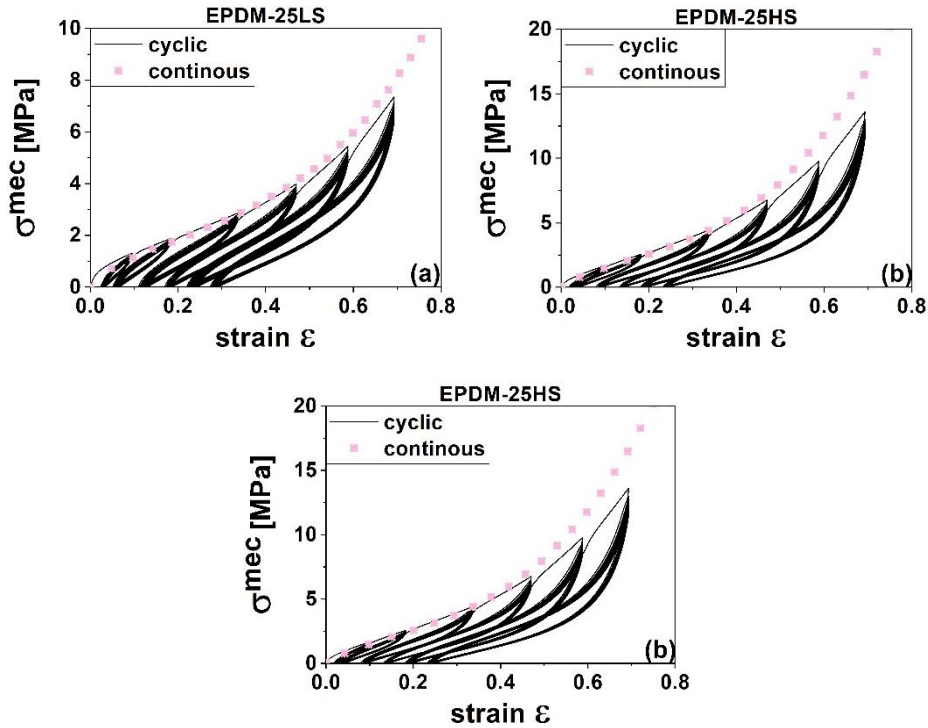


Figure 4. Continuous (cross lines) and cyclic (solid lines) stress-strain responses of a) EPDM-25LS b) EPDM-25HS c) EPDM-25HS.

In order to quantify the mechanical hysteresis, Fig. 5 displays R_M for the 1st, 5th and 50th cycle and the mechanical dissipated energy A_{mec} corresponding to different applied strains for nanocomposites with various CB contents (EPDM-25LS and EPDM-35LS) and different structures (EPDM-25LS and EPDM-25HS). For EPDM-25LS (Fig. 5a), the Mullins ratio R_M reaches 53.5 % at the first cycle for $\epsilon_{max} = 0.09$ and then rapidly decreases with increasing the number of cycles. The difference in R_M between the

5th and 50th cycle is only 3.8 %, attaining a rather steady value of ~ 30.8 % after the 5th cycle. This is in agreement with the fast mechanical stabilization observed in Fig. S8. The relatively high R_M during the 1st cycle and its reduction during subsequent cycles suggest that a reorganisation takes places, due to time-dependent stress relaxation [19] or interphase damage between EPDM and CB [20]. Nonetheless, R_M is almost constant for each 1st cycle in the strain range $0.09 < \varepsilon < 0.69$. $R_M = 53.7\%$ for $\varepsilon_{max} = 0.69$, which induces a variation of 0.2% between R_M at $\varepsilon_{max} = 0.69$ and R_M at $\varepsilon_{max} = 0.09$.

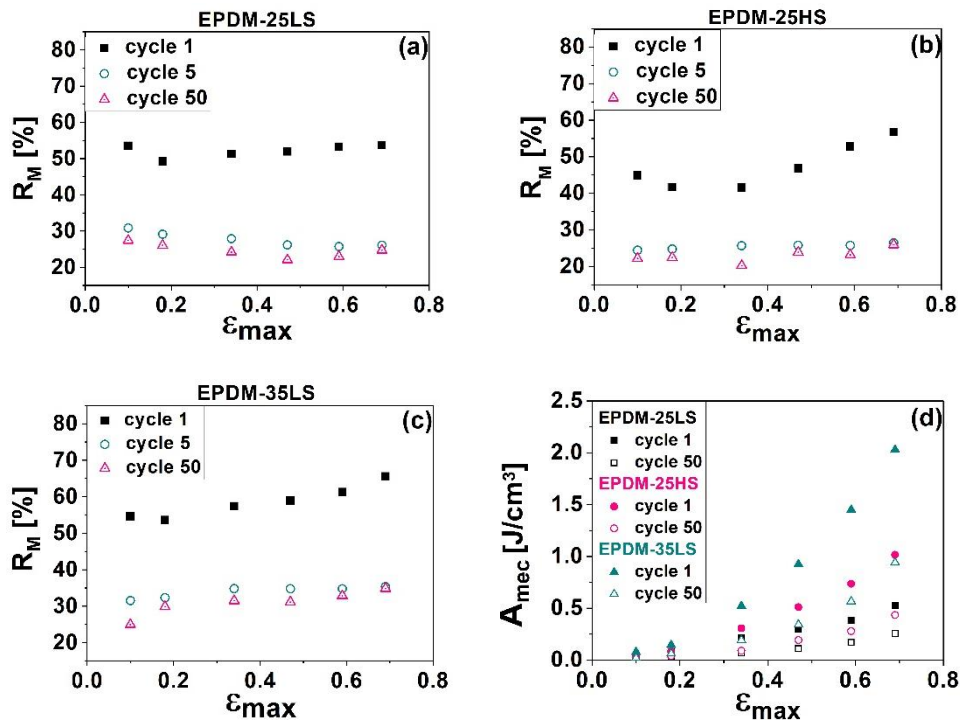


Figure 5. Mechanical hysteresis of a) EPDM-25LS b) EPDM-25HS c) EPDM-35LS during the 1st, 5th and 50th cycle as a function of ε_{max} and d) A_{mec} , corresponding to the dissipated energy for the 1st and the 50th cycle as a function of ε_{max} .

For the same content of HS CB, EPDM-25HS (Fig. 5b) shows an evolution with the number of cycles similar to that of EPDM-25LS. Yet, the initial value of R_M is lower and, starting from $\varepsilon_{max} = 0.34$ where $R_M = 41.6$ %, R_M increases with increasing ε . The difference between R_M at $\varepsilon_{max} = 0.34$ and at $\varepsilon_{max} = 0.69$ is 17.1 %. The hysteresis behaviour can be explained by considering the interactions at the polymer/filler interface

and the reorganisation of the filler aggregates. For CB of higher structure, the filler/polymer interface and filler/filler friction increase, contributing to the hysteresis behaviour at high deformations [21]. For elastomeric matrices filled with LS CB, the mechanical hysteresis increases with increasing the filler content, as shown in Fig. 5c, and this effect is more pronounced at high values of ε_{max} [22]. For all investigated composites, the mechanical hysteresis area is increasing with increasing ε_{max} , as reported in Fig. 5d. A_{mec} also increases with the CB content and structure.

3.2 Electrical Mullins effect

In the current section, the impact of the Mullins effect on the percolation of the CB network is investigated, through a coupled mechanical/electrical approach. Two important factors are taken into account: the influence of the deformation amplitude and the impact of unloading displacement rate. Typical true strain-time, stress-time and conductivity-stress curves of the composite materials investigated in our study are presented in Fig. 6. The measured curves during the first 5 cycles at each strain are shown. The true strain has been successively increased from 0.09 to 0.69 and 50 cycles have been carried-out for each strain value. As shown in Fig. 6, the conductivity-strain curves exhibit a local maximum of conductivity both during loading and unloading. At high strains, the conductivity maximum is observed only during unloading for EPDM-25HS and EPDM-35LS (Fig. 6b/Fig. 7b and Fig. 6c/Fig. 7c).

The impact of the maximum strain on the characteristic conductivity-strain response of EPDM/CB nanocomposites measured during cyclic loading is shown in Fig. 7, where the maximal strain was successively increased from 0.09, 0.18, 0.35, 0.47, 0.59 to 0.69. For EPDM-25LS, the electrical conductivity values during the mechanical cycles decrease with increasing ε_{max} . For a given cycle, the value of conductivity exhibits a

maximum both for the loading and unloading curve. Quantitatively comparing different cycles carried-out for EPDM-25LS, it is observed that the conductivity peak during unloading from $\varepsilon_{max} = 0.09$ is close to $\sigma_N^{elec} = 1.2 \cdot 10^{-3}$ S/cm, whereas $\sigma_N^{elec} = 4.1 \cdot 10^{-4}$ S/cm for $\varepsilon_{max} = 0.69$ (Fig. 7a). Thus, a reversible behaviour can be observed at small strains. This does not seem to be the case for higher ε , where the electrical behaviour appears to become irreversible, as shown by a hysteresis behaviour that increases with ε .

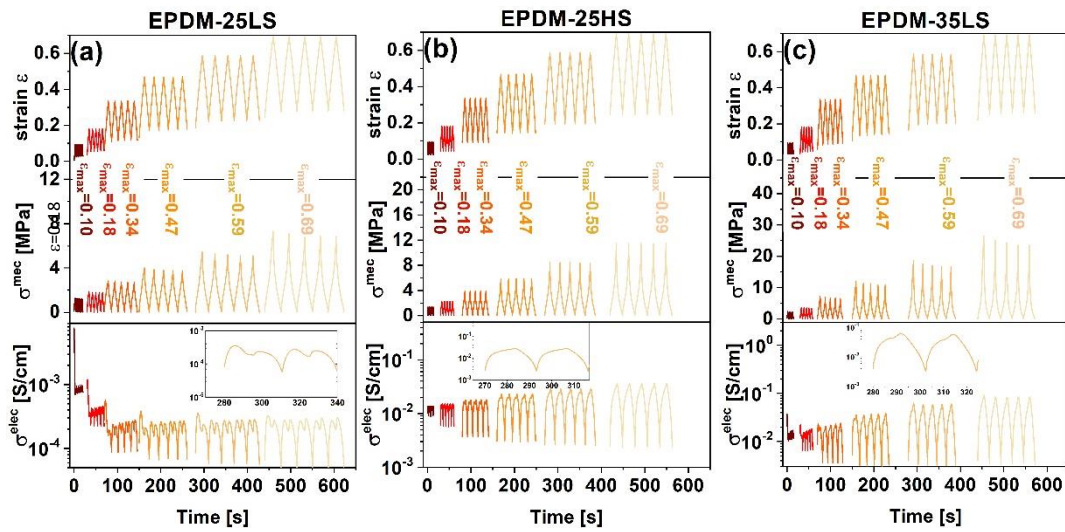


Figure 6. 5 first loading-unloading cycles where strain, stress and conductivity vs. time are reported for a) EPDM-25LS b) EPDM-25HS and c) EPDM-35LS for ε_{max} of 0.09, 0.18, 0.34, 0.47, 0.59 and 0.69. The insets are a zoom of the electrical response for 2 cycles at $\varepsilon_{max} = 0.59$.

σ^{elec} vs. ε plots at different amplitudes for EPDM-25HS and EPDM-35LS are reported in Fig. 7b and Fig. 7c. Contrarily to EPDM-25LS, the maximum value of conductivity during the mechanical cycles increases with increasing ε_{max} . The conductivity peaks during unloading are $\sigma_{N-25HS}^{elec} = 1.4 \times 10^{-2}$ S/cm and $\sigma_{N-35LS}^{elec} = 2.3 \times 10^{-2}$ S/cm for $\varepsilon_{max} = 0.09$, while the maximum of conductivity is $\sigma_{N-25HS}^{elec} = 3.7 \times 10^{-2}$ S/cm and $\sigma_{N-35LS}^{elec} = 8.6 \times 10^{-2}$ S/cm for $\varepsilon_{max} = 0.69$. The electrical hysteresis, quantified by the

parameter A_{elec} , becomes more important with increasing ε_{max} for EPDM-25HS and EPDM-35LS and stays almost constant for EPDM-25LS. This agrees with the evolution of A_{mec} , which is more pronounced for EPDM-25HS and EPDM-35LS (Fig. 5d). Nevertheless, the evolution of σ^{elec} during loading stays monotonic for EPDM-25HS and EPDM-35LS. During unloading, the $\sigma^{elec}-\varepsilon$ curves exhibit a well-defined maximum whose position varies linearly with ε_{max} . For EPDM-25HS at $\varepsilon_{max}=0.69$, σ^{elec} increases during loading.

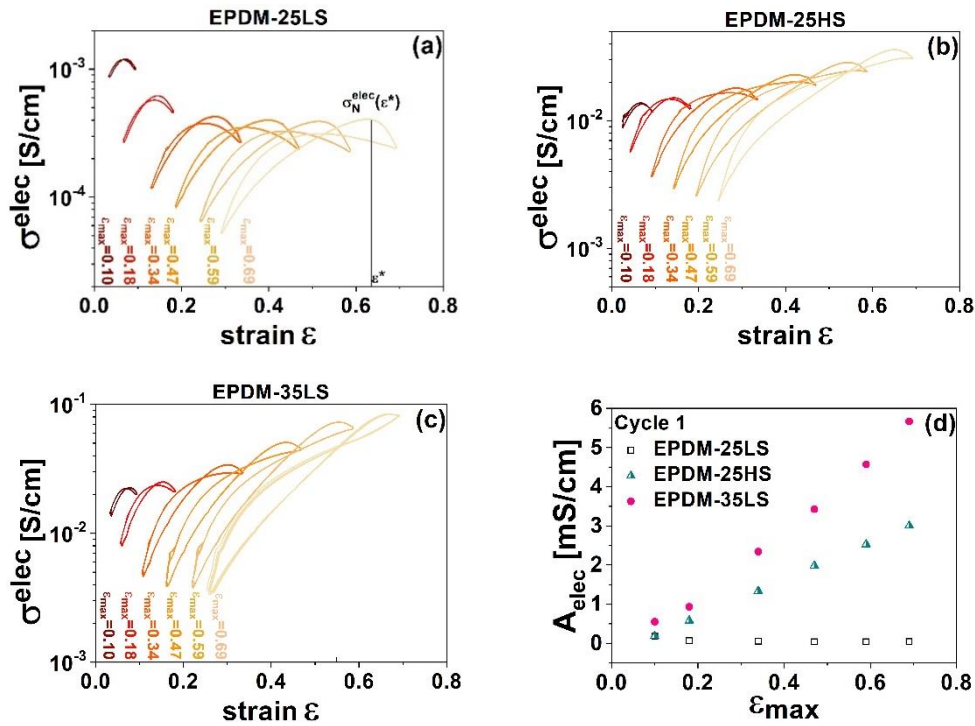


Figure 7. 5 last cycles of loading/unloading for ε_{max} of 0.09, 0.18, 0.34, 0.47, 0.59 and 0.69 are shown for a) EPDM-25LS b) EPDM-25HS and c) EPDM-35LS. 50 cycles are carried-out for each amplitude d) A_{elec} as a function of ε_{max} for the 1st cycle.

A notable difference between the electrical and mechanical hysteresis can be distinguished: the loading/unloading conductivity curves cross each other while this is not the case for the mechanical results. For instance, during the unloading after reaching $\varepsilon = 0.67$, the conductivity decreases and become smaller than the conductivity during

loading. The equilibrium electrical behaviour of all investigated EPDM/CB composites for $\varepsilon_{max} = 0.69$ is reported in Fig. S9. The phenomenon of electric hysteresis appears thus to be more complex than the mechanical one. A non-monotonic electrical response under cyclic loading has been previously reported in the literature [15,19,23–25]. Several theories based on electron tunnelling effects and creation/destruction of conductive network indicate that the conductivity decreases under stretching due to filler-to-filler separation [26]. Conventionally, during the unloading cycle, the conductivity increases by the reduction in the filler/filler distance which increases the number of conductive paths [14,27]. Disorder effects of the polymer chains and of the CB network could also contribute to this behaviour, as proposed by Aneli et al. [28]. Another aspect to be considered is related to the fact that, throughout the loading the strain increases and the width and thickness of the sample decreases, reducing thereby the distance between the CB aggregates in the transverse direction.

As in the mechanical Mullins effect, the electrical behaviour during the 1st loading is markedly different than in the following loading cycles (Fig. 8). This effect is more pronounced for EPDM-25LS, as compared to the other composites (Fig. 8a). The phenomenon of electrical hysteresis indicates that the percolation of the CB network is not the same during the loading and unloading steps. The non-monotonic and hysteresis effects can be thus related to a competing interplay of connecting/disconnecting electrical pathways occurring due to the axial and perpendicular deformation.

During cyclic deformations at low strains ($\varepsilon_{max} < 0.15$), all composite materials investigated in our study display a maximum in the σ^{elec} - ε plots and a low hysteresis. Loading will first induce new filler-filler contacts due to the negative deformation in the perpendicular direction and thus an increase of conductivity. Above the maximal conductivity threshold (that depends on the maximal applied strain), loose contacts or separation of CB particles and aggregates resulting from the axial positive deformation

will dominate the electrical behaviour, leading to a decrease of conductivity. This behaviour appears to be reversible with decreasing the axial ε during unloading. For larger applied axial ε ($\varepsilon_{max} > 0.15$), unloading still displays a conductivity maximum that systematically appears at a higher ε than upon loading.

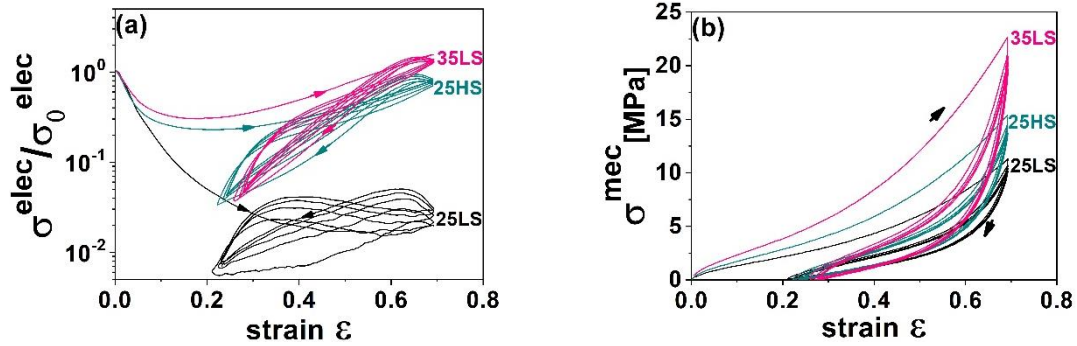


Figure 8. 5 first cycles out of 50 cyclic loading a) Normalized conductivity according to the initial electrical conductivity σ_0 as a function of strain b) stress-strain response.

Reconnecting the CB fillers along the axial direction by reduction of inter-particle distance appears to be a faster process than the competing mechanism taking place in the perpendicular direction and leading to disconnection of the particles/aggregates by the evolution of the perpendicular ε . This indicates that the configuration of the CB network evolves with both axial and perpendicular ε , according to the CB structure and applied maximal strain ε_{max} . Such difference in the axial and perpendicular restructuring dynamics results from the interactions between the rubber matrix and the filler as well as from the non-elastic deformation within the confined polymer matrix [28]. The conductivity peaks, related to the points in the $\sigma^{elec} - \varepsilon$ plots where the creation of new conductive pathways in one direction (axial or transverse) compensates the destruction of the percolation network in the other direction, clearly depend on the applied ε as well as on the CB structure and concentration. To fully explain the observed phenomena, a simulation of tri-dimensional (axial and transverse) motions of the CB aggregate network could be very helpful, but it is still challenge to provide accurate insights [29].

In order to confirm the percolation/de-percolation/re-percolation mechanisms taking place parallel and perpendicular to the stretching direction, in-situ coupled Small Angle X-Ray Scattering experiments have been carried-out in our study, to analyse the structural changes of our materials upon mechanical deformation. Our SAXS data reveal a anisotropic structural evolution (evidenced by the formation of a butterfly-like SAXS pattern) appearing during mechanical stretching and indicating a filler/filler distance that becomes shorter in the perpendicular direction, favouring thereby the electrical percolation (Fig. S10a,b,c in the Supplementary Information). This finding is fully coherent with the CB reorganisation mechanism proposed in our study. Furthermore, by comparing the SAXS data obtained upon loading and unloading at the same deformation amplitude, a structural hysteresis is clearly evidenced as well (Fig. S10d,e in the Supplementary Information), in full agreement with the electrical and mechanical hysteresis observed in our coupled measurements.

The electrical hysteresis plots normalized by the initial conductivity σ_0 are presented in Fig. 8, for a fixed $\varepsilon_{max}=0.69$. Fig. 8a illustrates the 5 first cycles of σ^{elec} vs. ε at $\varepsilon_{max}=0.69$, and Fig. 8b displays the normalized ε vs. σ^{mec} curves. During the first loading, the conductivity starts to decrease with increasing ε (Fig. 8a) and then increases above $\varepsilon > 0.2$ (for EPDM-25HS and EPDM-35LS), displaying thus a minimum in conductivity. On contrary, during the subsequent cycles, a conductivity maximum is observed during unloading. As in the mechanical response (Fig. 8b), the first loading exhibits a specific electrical response as compared to the following cycles. Similarly to the mechanical results, the σ^{elec} vs ε curves show a hysteresis behaviour: the conductivity evolution during loading is different from the one during unloading. Thus, similarly to the classical mechanical Mullins effect, the coupled electrical response of all investigated materials measured during mechanical deformation exhibits also an electrical Mullins effect, with a specific electrical signature. Notable differences between the mechanical

and the electrical Mullins effects can be however observed. For instance, the evolution of electrical conductivity takes significantly more than 5 cycles before settling to an equilibrated loop. In this sense, the conductivity seems to be considerably more time dependent than the σ^{mec} .

In order to further compare the number of cycles necessary to reach the equilibrium state for the electrical and mechanical cyclic loops, Fig. 9 reports the maximum stress amplitude $\sigma_{max,N}^{meca} / \sigma_{max,N=0}^{meca}$ as a function of the cycle number N (Fig. 9a) and the conductivity at the unloading peak normalized by the initial amplitude of conductivity $\sigma_{max,N}^{elec} / \sigma_{max,N=0}^{elec}$ as a function of N (Fig. 9b). As shown in Fig. 9a, **the mechanical stabilization is reached in less than 10 cycles for all investigated materials. However, this is not the case for the electrical response, that needs a longer time to reach the equilibrium state (Fig. 9b).**

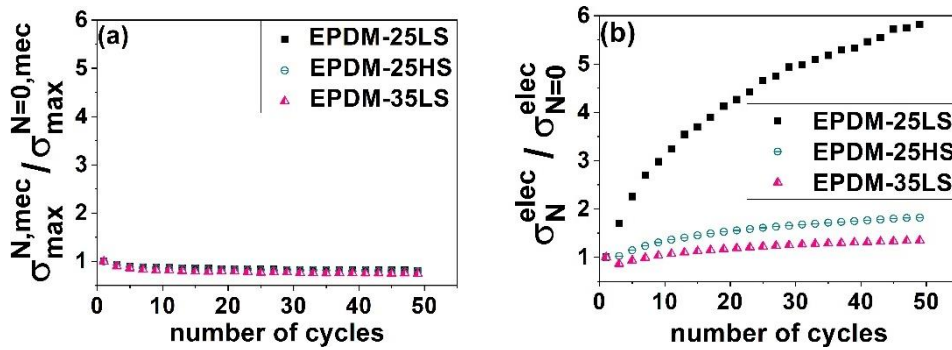


Figure 9. a) Evolution of the maximum of stress amplitude $\sigma_{max,N}^{meca} / \sigma_{max,N=0}^{meca}$ with the number of cycles b) Evolution of the conductivity amplitude σ_N^{elec} of the composite normalized by the initial amplitude $\sigma_{N=0}^{elec}$ with the number of cycles.

Another important parameter to be considered in the analysis of the Mullins effects is the unloading displacement rate, playing a major role in the reorganisation kinetics of the percolated CB network. The differences in the loading and unloading curves observed in the measured data arise from a tri-dimensional dynamic rearrangement

of the CB network induced by the mechanical stretching. Relaxation phenomena of the polymer matrix play obviously an important role, too. In order to investigate their impact on the coupled mechanical/electrical behaviour of EPDM/CB composite materials, measurements at a constant loading rate of ($v_{loading} = 10$ mm/min) but at different unloading displacement rates ($v_{unloading}$ of 0.5 mm/min, 10 mm/min, 50 mm/min and 500 mm/min) have been carried-out. The results are reported in Fig. 10 for EPDM-25LS.

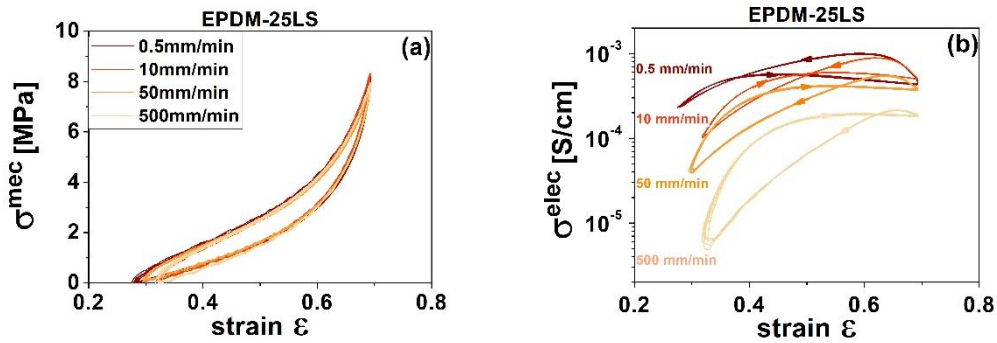


Figure 10. 5 last cycles (out of 50 strain cycles) showing a) stress-strain response b) conductivity-strain responses for EPDM-25LS at various $v_{unloading}$.

The mechanical Mullins effect is not significantly affected by the variation of the unloading rate $v_{unloading}$, except for a small non-recovered ϵ at the end of the unloading step at $\sigma^{mech}=0$, increasing, as expected, with the unloading rate. The kinetics of the strain recovery appears to be faster as compared to the applied unloading rates, in agreement with a highly cross-linked matrix that exhibits a strong elastic recovery. On contrary, the electrical Mullins effect is highly dependent on the unloading displacement rate (Fig. 10b). When $v_{unloading} < v_{loading}$, the σ^{elec} -vs ϵ electrical response for $0.25 < \epsilon_{max} < 0.35$ is the same during loading and unloading, almost no electrical Mullins hysteresis being detected in this range. For $0.35 < \epsilon_{max} < 0.69$ a hysteresis becomes noticeable, with conductivity upon unloading systematically higher than the conductivity upon loading. When $v_{unloading} > v_{loading}$ (i.e. $v_{unloading}$ set to 50 mm/min or 500 mm/min) the hysteresis is more pronounced for $0.30 < \epsilon < 0.69$. In comparison to low

$v_{unloading}$ conditions, the conductivity maximum is obtained at a higher ε and the unloading curve generally remains well below the loading curve. Thus, at high values of $v_{unloading}$, the re-percolation of the CB network is less developed, due to the limited time imposed by the fast unloading rate. This results in a lower conductivity value and higher conductivity variation during one cycle (up to 2 decades). The σ^{elec} evolution with ε is thus proven to be considerably sensitive to the deformation rates. This is partly due to the anelasticity of the polymer matrix implied in the restructuration of the CB network during the loading and unloading. Since limited variations of the Mullins effect were noticed under the same conditions, it may be concluded that the electrical Mullins hysteresis is due to slower/larger scale microstructural reorganisation events. Thus, the matrix anelasticity strongly affects the destruction/reconstruction of the 3D CB network electrical percolation during cyclic loading, the apparent crosslinking density of the composites being less affected.

4. Conclusions

In this work, in-situ coupled mechanical/electrical investigations upon cyclic and continuous loading on EPDM-based composite materials prepared using CB fillers of different (low and high) structure and at different concentrations have been carried-out. The coupled mechanical/electrical measurements have been performed in systematic dependence on the strain amplitude and unloading displacement rate. A clear electrical signature of the mechanical Mullins effect is revealed in the curves of electrical conductivity vs. mechanical strain. As in the mechanical Mullins effect, the electrical Mullins effect exhibits a strong dependence of the deformation history of the investigated materials. Non-monotonic electrical conductivity/mechanical strain curves accompanied by a phenomenon of electric hysteresis are observed, indicating a reorganisation of the

CB percolation upon loading and unloading. This reorganisation of the CB fillers is driven by competing mechanisms of de-percolation and re-percolation taking place parallel and perpendicular to the stretching direction. The electrical hysteresis depends on the applied strain but also on the relaxation kinetics of the polymer matrix. This is clearly demonstrated by performing unloading experiments at different displacement rates between 0.5 mm/min and 500 mm/min. It is shown that, unlike the mechanical Mullins effect, the electrical Mullins effect strongly depends on the unloading displacement rate. This is due to a kinetics of re-percolation that is becoming too slow compared to the unloading rate. Our study brings new light into the understanding of the Mullins effect, by revealing, through in-situ coupled mechanical/electrical investigations, a different facet of this phenomenon related to a kinetic reorganisation of the fillers upon mechanical deformation. This could be of potential interest in numerous applications for monitoring the evolution of mechanical properties of elastomeric materials by in-situ coupled electrical measurements.

Acknowledgements: The financial support given by ANRT through the CIFRE project no. 0479-0065 is highly acknowledged.

References

- [1] X. Guo, Y. Huang, X. Cai, C. Liu, P. Liu, Capacitive wearable tactile sensor based on smart textile substrate with carbon black/silicone rubber composite dielectric, *Meas. Sci. Technol.* 27 (2016) 045105.
- [2] J.J.C. Busfield, C. Deprasertkul, A.G. Thomas, The effect of liquids on the dynamic properties of carbon black filled natural rubber as a function of pre-strain, *Polymer*. 41 (2000) 9219–9225.
- [3] K. Tsunoda, J.J.C. Busfield, C.K.L. Davies, A.G. Thomas, Effect of materials

variables on the tear behaviour of a non-crystallising elastomer, *Journal of Materials Science*. 35 (2000) 5187–5198.

[4] J. Busfield, A. Muhr, *Constitutive Models for Rubber III: Proceedings of the Third European Conference on Constitutive Models for Rubber*, London, UK, 15-17 September 2003, CRC Press, 2003.

[5] L. Karásek, B. Meissner, S. Asai, M. Sumita, *Percolation Concept: Polymer-Filler Gel Formation, Electrical Conductivity and Dynamic Electrical Properties of Carbon-Black-Filled Rubbers*, *Polymer Journal*. 28 (1996) 121–126.

[6] S.-J. Park, K.-S. Cho, S.-K. Ryu, *Filler–elastomer interactions: influence of oxygen plasma treatment on surface and mechanical properties of carbon black/rubber composites*, *Carbon*. 41 (2003) 1437–1442.

[7] P. Buckley, *Experimental Methods for Rubberlike Solids*, in: G. Saccomandi, R.W. Ogden (Eds.), *Mechanics and Thermomechanics of Rubberlike Solids*, Springer, Vienna, 2004: pp. 1–62.

[8] L. Mullins, *Effect of Stretching on the Properties of Rubber*, *Rubber Chemistry and Technology*. 21 (1948) 281–300.

[9] L. Mullins, N.R. Tobin, *Theoretical Model for the Elastic Behavior of Filler-Reinforced Vulcanized Rubbers*, *Rubber Chemistry and Technology*. 30(1957)555–571.

[10] J. Diani, B. Fayolle, P. Gilormini, *A review on the Mullins effect*, *European Polymer Journal*. 45 (2009) 601–612.

[11] N. Ning, C. Miao, H. Zou, Q. Shao, S. Wang, L. Zhang, M. Tian, *A new insight on the variation of the electric conductivity and conductive network of silver-coated glass particles/silicone elastomer composites under tensile strain*, *Composites Science and Technology*. 136 (2016) 46–52.

[12] C. Cattin, P. Hubert, *Piezoresistance in Polymer Nanocomposites with High Aspect Ratio Particles*, *ACS Appl. Mater. Interfaces*. 6 (2014) 1804–1811.

- [13] C. Su, L. Xu, C. Zhang, J. Zhu, Selective location and conductive network formation of multiwalled carbon nanotubes in polycarbonate/poly(vinylidene fluoride) blends, *Composites Science and Technology*. 71 (2011) 1016–1021.
- [14] J. Zhu, S. Wei, J. Ryu, Z. Guo, Strain-Sensing Elastomer/Carbon Nanofiber “Metacomposites,” *J. Phys. Chem. C*. 115 (2011) 13215–13222.
- [15] D.S.A.D. Focatiis, D. Hull, A. Sánchez-Valencia, Roles of prestrain and hysteresis on piezoresistance in conductive elastomers for strain sensor applications, *Plastics, Rubber and Composites*. 41 (2012) 301–309.
- [16] J. Zhao, K. Dai, C. Liu, G. Zheng, B. Wang, C. Liu, J. Chen, C. Shen, A comparison between strain sensing behaviors of carbon black/polypropylene and carbon nanotubes/polypropylene electrically conductive composites, *Composites Part A: Applied Science and Manufacturing*. 48 (2013) 129–136.
- [17] S. Zheng, J. Deng, L. Yang, D. Ren, W. Yang, Z. Liu, M. Yang, A highly-deformable piezoresistive film composed of a network of carbon blacks and highly oriented lamellae of high-density polyethylene, *RSC Advances*. 5 (2015) 31074–31080.
- [18] H. Liu, Y. Li, K. Dai, G. Zheng, C. Liu, C. Shen, X. Yan, J. Guo, Z. Guo, Electrically conductive thermoplastic elastomer nanocomposites at ultralow graphene loading levels for strain sensor applications, *Journal of Materials Chemistry C*. 4 (2016) 157–166.
- [19] C. Lozano-Pérez, J.V. Cauich-Rodríguez, F. Avilés, Influence of rigid segment and carbon nanotube concentration on the cyclic piezoresistive and hysteretic behavior of multiwall carbon nanotube/segmented polyurethane composites, *Composites Science and Technology*. 128 (2016) 25–32.
- [20] T.-T. Mai, Y. Morishita, K. Urayama, Novel features of the Mullins effect in filled elastomers revealed by stretching measurements in various geometries, *Soft Matter*. 13 (2017) 1966–1977.
- [21] M. Pingot, B. Szadkowski, M. Zaborski, Effect of carbon nanofibers on mechanical

and electrical behaviors of acrylonitrile-butadiene rubber composites, *Polymers for Advanced Technologies*. 29 (2018) 1661–1669.

[22] W. Fu, L. Wang, J. Huang, C. Liu, W. Peng, H. Xiao, S. Li, Mechanical Properties and Mullins Effect in Natural Rubber Reinforced by Grafted Carbon Black, *Advances in Polymer Technology*. 2019 (2019) e4523696.

[23] H. Yang, X. Yao, L. Yuan, L. Gong, Y. Liu, Strain-sensitive electrical conductivity of carbon nanotube-graphene-filled rubber composites under cyclic loading, *Nanoscale*. 11 (2019) 578–586.

[24] L. Duan, S. Fu, H. Deng, Q. Zhang, K. Wang, F. Chen, Q. Fu, The resistivity–strain behavior of conductive polymer composites: stability and sensitivity, *J. Mater. Chem. A*. 2 (2014) 17085–17098.

[25] V. Kumar, G. Lee, K. Singh, J. Choi, D.-J. Lee, Structure-property relationship in silicone rubber nanocomposites reinforced with carbon nanomaterials for sensors and actuators, *Sensors and Actuators A: Physical*. 303 (2020) 111712.

[26] C. Brosseau, A. Mdarhri, A. Vidal, Mechanical fatigue and dielectric relaxation of carbon black/polymer composites, *Journal of Applied Physics*. 104 (2008) 074105.

[27] M.K. Shin, J. Oh, M. Lima, M.E. Kozlov, S.J. Kim, R.H. Baughman, Elastomeric Conductive Composites Based on Carbon Nanotube Forests, *Advanced Materials*. 22 (2010) 2663–2667.

[28] J.N. Aneli, G.E. Zaikov, L.M. Khananashvili, Effects of mechanical deformations on the structurization and electric conductivity of electric conducting polymer composites, *Journal of Applied Polymer Science*. 74 (1999) 601–621.

[29] J. Liu, L. Zhang, D. Cao, J. Shen, Y. Gao, computational simulation of elastomer nanocomposites: current progress and future challenges, *Rubber Chemistry and Technology*. 85 (2012) 450–481.